Secondary reactions of aromatics-derived oxygenated organic molecules lead to plentiful highly oxygenated organic molecules within an intraday OH exposure

Yuwei Wang[1], Yueyang Li[1], Gan Yang[1], Xueyan Yang[1], Yizhen Wu[1], Chuang Li[1], Lei Yao[1,2], Hefeng Zhang[3*], Lin Wang[1,2,4,5,6] *

[1] Shanghai Key Laboratory of Atmospheric Particle Pollution and Prevention (LAP[3]), Department of Environmental Science and Engineering, Jiangwan Campus, Fudan University, Shanghai 200438, China

[2] Shanghai Institute of Pollution Control and Ecological Security, Shanghai 200092, China

[3] State Environmental Protection Key Laboratory of Vehicle Emission Control and Simulation, Vehicle Emission Control Center of Ministry of Ecology and Environment, Chinese Research Academy of Environmental Sciences, Beijing 100012, China

[4] IRDR International Center of Excellence on Risk Interconnectivity and Governance on Weather/Climate Extremes Impact and Public Health, Fudan University

[5] National Observations and Research Station for Wetland Ecosystems of the Yangtze Estuary, Shanghai, China

[6] Collaborative Innovation Center of Climate Change, Nanjing, 210023, China

Corresponding Author: H.Z., email, zhanghf@craes.org.cn; phone, +86-10-84915586
L.W., email, lin_wang@fudan.edu.cn; phone, +86-21-31243568

ABSTRACT. Highly oxygenated organic molecules (HOMs) can participate in new particle formation (NPF) and enhance growth of newly formed particles partially because of their low volatility. Previous studies have shown formation of HOMs via autoxidation reactions of RO_2 intermediates generated by OH-initiated oxidation of anthropogenic volatile organic compounds (VOCs). It was also suggested that multi-generation OH oxidation could be an important source for aromatics-derived HOMs. However, our understanding on the generation of aromatics-derived HOMs are still insufficient, especially for their formation mechanisms, which determine molar yields of HOMs and are essential to the establishment of global chemical box models related to HOMs. In this study, with a potential aerosol formation oxidation flow reactor (PAM OFR), a series of OH-initiated oxidation experiments of 1,3,5-trimethylbenzene (1,3,5-TMB) were conducted to investigate the influences of the extent of OH exposure on the formation of aromatics-derived HOMs. The evolution of oxidation products of 1,3,5-TMB in an OH exposure range of $(0.5 - 5.0) \times 10^{10}$ molecules cm^{-3} s, equivalent to an OH exposure of 0.7 – 6.9 hours at an OH concentration of 2×10^6 molecules cm^{-3}, was investigated by a nitrate-based chemical ionization mass spectrometer and a Vocus proton-transfer-reaction mass spectrometer, indicating significant secondary OH chemistry

37   during the ageing of stabilized first generation oxygenated products within an intraday OH

38   exposure and formation of various HOMs with more oxygen content and thus lower volatility.

39   In addition, organonitrates, formed after the introduction of NO_x into the reaction systems,

40   further confirmed the existence of such secondary reactions. Our study suggests an important

41   role of secondary OH chemistry in the oxidation of aromatics and elucidates detailed formation

42   mechanisms of certain HOM products.

43

44   **1 Introduction**

45   OH radicals can react with volatile organic compounds (VOCs) in the atmosphere,

46   converting primary pollutants to secondary ones. Generated from oxidation of VOCs,

47   oxygenated organic molecules (OOMs) are crucial in a variety of atmospheric chemical

48   processes, contributing efficiently to the formation of secondary organic aerosols (SOAs) and

49   ground-level O_3 (Ng et al., 2010; Qu et al., 2021; Wang et al., 2022). Among the enormous

50   number of oxygenated VOCs (OVOCs), highly oxygenated organic molecules (HOMs) have

51   recently attracted significant attention (Bianchi et al., 2019). Most of HOMs are low volatile

52   organic compounds (LVOCs) or extremely low volatile organic compounds (ELVOCs), and

53   thus are able to drive the initial formation of nucleated particles under certain conditions and

54   contribute to the subsequent growth of newly-formed particles, which finally enhance SOA

55   formation (Lehtipalo et al., 2018; Mohr et al., 2019; Qiao et al., 2021; Stolzenburg et al., 2018;

56   Tröstl et al., 2016).

57   Formation of HOMs is typically triggered by oxidation of VOCs in the gas phase. Peroxy

58   radicals (RO_2) are generated at the initial step and will undergo an intramolecular hydrogen

59   atom shift forming a hydroperoxide functionality and an alkyl radical. A molecular oxygen will

60   rapidly attach to this alkyl radical and form a new and more oxidized RO_2. This reaction is

61   called as autoxidation and the newly formed RO_2 can go through another autoxidation or

62   bimolecular termination reactions to form a stabilized product (Crounse et al., 2013).

63   Autoxidation is suggested to be responsible for widely detected HOMs in the atmosphere,

64   because it can form highly oxygenated RO_2 in a short time scale. In terms of biomolecular

65   reactions, RO_2 reacts appreciable only with hydroperoxyl radical (HO_2), NO, and another RO_2.

66   The RO_2 reaction chain in polluted areas is largely terminated by NO, which prohibits

67   generation of compounds with high oxidation levels and reduces yields of HOMs (Bianchi et

68   al., 2019).

69   Nevertheless, autoxidation reactions alone are not enough to explain the large numbers of

70   oxygen atoms in HOMs observed in laboratory experiments and ambient campaigns. Take

71   alkylbenzenes as an example, previous studies suggest that the main products of OH oxidation

72   of alkylbenzenes (C_xH_{2x-6}, x=7, 8, or 9), i.e., bicyclic peroxy radicals (BPR, $C_xH_{2x-6}O_5{\cdot}$, x=7, 8,

73   or 9), can undergo an autoxidation reaction and form a new peroxy radical, $C_xH_{2x-6}O_7{\cdot}$ (x=7, 8,

74   or 9) (Jenkin et al., 2003). The autoxidation reaction of BPR could be very fast because an

75   allylic radical will be formed after the hydrogen shift (Wang et al., 2017). On the other hand,

76   the structure of resulting $C_xH_{2x-6}O_7{\cdot}$ is strongly different from that of BPR, whose autoxidation

77   reaction rate can be as low as the order of 0.001 s^{-1}, since it lacks enhancements from favorable

78   transition state geometries and substitutes or resonance structures (Bianchi et al., 2019; Otkjær

79   et al., 2018). Such a slow autoxidation reaction rate cannot explain the extensive existence of

80   HOM monomers with more than 7 oxygen atoms and HOM dimers with more than 10 oxygen

81   atoms, which are the maximum numbers of oxygen atoms in stabilized monomer and dimer

82   products, respectively, formed from $C_xH_{2x-6}O_7{\cdot}$ (Mentel et al., 2015; Molteni et al., 2018; Wang

83   et al., 2020). Another possibility is the formation of a second oxygen bridge after the hydrogen

84   shift of BPR (Molteni et al., 2018), but this reaction pathway would not allow a further

85   oxygenation reaction without a breakage of the carbon ring, which is also unpromising.

86   Multigeneration reactions of VOCs complicate HOMs' formation. Previous studies

87   indicate that HOMs can also be formed by sequential oxidation of stabilized first-generation

88   products of benzene and toluene (Cheng et al., 2021; Garmash et al., 2020). Garmash et al.

89   (2020) conducted OH oxidation experiments of benzene and toluene with an OH exposure

90   equivalent to atmospheric oxidation times of 10 hours – 15 days at OH concentrations of $\sim 10^6$

91   molecules cm^{-3}. Cheng et al. (2021) simulated oxidation of benzene and toluene with an OH

92   exposure equivalent to 2.4 – 19.4 days of atmospheric photochemical ageing. Certainly, such

93   extremely high OH exposures favor secondary OH chemistry and help to facilitate our

94   understanding on product distributions, but such a long timescale limits atmospheric

95   implications of their results, given the complex physical and chemical processes at night.

96   Compared to benzene and toluene, trimethylbenzene (TMB) is a precursor characterized

97   with much larger HOM molar yields when reacted with OH, and the abundance of TMB in the

98   atmosphere is unignorable (Molteni et al., 2018; Yuan et al., 2012). Previous laboratory

99   experiments on TMB-derived HOMs mainly focused on the autoxidation reactions of BPR and

100   the influences of NO_x, while the quantity of experiments was finite with a limited range of OH

101   exposure, bringing down the universality and applicability of conclusions (Tsiligiannis et al.,

102   2019; Wang et al., 2020). From the mechanism perspective, a number of HOM monomers with

103   more than 7 oxygen atoms detected in the OH-initiated oxidation of TMB were previously

104   assumed to be generated via multiple autoxidation reactions (Molteni et al., 2018). Nevertheless,

105   a subsequent OH oxidation of the first-generation oxygenated products might be more plausible

106   for the formation of HOM monomers with more than 7 oxygen atoms from the present point of

107   view. Indeed, laboratory experiments show that RO_2 formed during the second-generation OH

108   oxidation of the first-generation stabilized oxidation products can also undergo autoxidation

109   reactions, which entangles reaction mechanisms potentially involved in the formation of those

110   HOMs and justifies more investigations on the multigeneration OH oxidation of aromatics

111   (Wang et al., 2020). High atmospheric concentrations of OH have been frequently observed in

112   both urban and suburban environments in China (Lu et al., 2012; Tan et al., 2019), leading to a

113   realistic implication of multigeneration OH oxidation. Therefore, it is imperative to study

114   chemical characteristics of formation reactions of HOMs at different OH exposures, especially

115   those fewer than or equivalent to one day of atmospheric oxidation.

116   In this study, a series of laboratory experiments were conducted on the OH-initiated

117   oxidation of 1,3,5-TMB, selected as an example of anthropogenic VOCs with an OH exposure

118   equivalent to atmospheric oxidation times of roughly 0.7 – 6.9 hours at an average daytime OH

119   radical concentration of 2.0×10^6 molecules cm^{-3}. A nitrate-based chemical ionization mass

120   spectrometer (nitrate CIMS) and a Vocus proton-transfer-reaction mass spectrometer (Vocus

121   PTR) were deployed to measure the oxidation products and the precursor, respectively. From

122   the evolution of oxygenated products, we explored secondary OH chemistry of stabilized first-

123   generation oxygenated products generated by the oxidation of 1,3,5-TMB. Furthermore, the

124   influence of NO on the formation of HOMs was investigated by introducing N_2O into the

125   reaction system via formation of organonitrates.

126

2 Methods

128   OH-initiated oxidation of 1,3,5-TMB was investigated in a potential aerosol formation

129   oxidation flow reactor (PAM OFR) system at $T = 298 \pm 1$ K and a pressure of 1 atm (Lambe et

130   al., 2015). The experimental settings in this study differed slightly from what were used

131   previously (Wang et al., 2020). Forty OH experiments (Exp. 1 – 40) and twenty-eight NO_x

132   experiments (Exp. 41 – 68) were performed, the experimental conditions of which are

133   summarized in Table S1, including concentrations of the precursor, ozone, and NO and NO_2.

134   The equivalent OH exposure in the OFR for each experiment was estimated according to the

135   precursor consumption, also listed in Table S1. OH exposures in the OFR were in the range of

136     $(0.5 – 5.0) \times 10^{10}$ molecules cm^{-3} s, equivalent to atmospheric oxidation times of roughly 0.7 –

137   6.9 hours for 1,3,5-TMB at an average daytime OH radical concentration of 2.0×10^6 molecules

138   cm^{-3}. In contrast, the OH oxidation lifetime for 1,3,5-TMB is around 2.4 hours at the

139   aforementioned atmospheric average daytime OH concentrations.

140   A home-made 1,3,5-TMB/N_2 cylinder was used as a stable gaseous precursor source in the

141   experiments, from which the flow rate of 1,3,5-TMB/N_2 varied between 1 – 3 sccm (standard

142 cubic centimeter per minute, standard to 0 °C, 1 atm), leading to 28.9 – 62.7 ppb of 1,3,5-TMB

143 in the OH oxidation experiments (Table S1). A total flow of 15 slpm (standard liters per minute,

144 standard to 0 °C, 1 atm) zero-gas generated by a zero-gas generator (model 737-13, Aadco

145 Instruments Inc.), together with the 1,3,5-TMB/N_2 flow, was introduced into the OFR. The

146 reaction time in this series of experiments was kept at around 53 s. The flow in the PAM OFR

147 is laminar with a very low axial mixing, as characterized with a Taylor dispersion model in a

148 previous study (Lambe et al., 2011). Among the 15 slpm zero-gas, 6 slpm was initially passed

149 through a Nafion humidifier (Perma Pure Model FC100-80-6MSS) filled with ultra-pure water

150 and finally converged with the main flow into the OFR to achieve and keep a desired RH of

151 20.0 ± 2.5 % in the OFR throughout all the experiments, and 2 slpm was initially passed through

152 a separate ozone chamber, resulting in an initial ozone concentration of around 429 – 881 ppb

153 in the OFR. The OFR was operated with only the 254 nm lights on, under which the primary

154 oxidant production reactions in the OFR were $O_3 + hv\,(254\,nm) \rightarrow O_2 + O(^1D)$ and

155 $O(^1D) + H_2O \rightarrow 2OH$. An ozone monitor (Model 106-M, 2B technologies) and a trace-gas

156 analyzer for NO-NO_2-NO_x (Thermo, 42i-TL) were placed at the exit of the OFR to measure

157 concentrations of ozone and NO_x, respectively.

158 For experiments with NO_x, 350 sccm N_2O (99.999%, Air Liquid) was added into the OFR

159 to produce and sustain NO_x mixing ratios at levels that were sufficiently high to be a competitive

160 sink for RO_2 radicals. NO and NO_2 were produced via the reaction $N_2O + O(^1D) \rightarrow 2NO$,

161 followed by the reaction $NO + O_3 \rightarrow NO_2 + O_2$. Two sets of irradiance intensities were chosen

162 for NO_x experiments, generally resulting in two NO_x levels, 1.8 ppb NO + 70 ppb NO_2 (Exp.

163 41 – 54) and 4.8 ppb NO + 120 ppb NO_2 (Exp. 55 – 68) at the exit of the OFR. With the aim to

164 slightly modify OH exposure but keep NO_x concentrations constant among each set of

165 experiments, the initial concentrations of 1,3,5-TMB were adjusted in a large range (16.7 – 84.1

166 ppb), as an increase in the precursor concentration corresponds to a larger sink for OH, while

167 RH and irradiances were not changed.

168 A nitrate CIMS (Ehn et al., 2014; Eisele and Tanner, 1993) and a Vocus PTR (Krechmer

169 et al., 2018) were deployed at the exit of the OFR to measure the oxidation products of 1,3,5-

170 TMB. These two mass spectrometers have been well characterized in a previous study (Wang

171 et al., 2020).

172 In this study, the sample flow rate for the nitrate CIMS was 8 slpm through a Teflon tube

173 with an outer diameter (OD) of 1/4 in. and a length of 70 cm. The sheath flow for the nitrate

174 CIMS was supplied by a zero-gas generator at a flow rate of 15 slpm. Mass resolution was

175 approximately 8000 for ions with m/z larger than 200 Th. HOMs generated from TMB

176 oxidation were charged in the ambient pressure interface region by collisions with nitrate

177   clusters, $(HNO_3)_x \cdot NO_3^-$ ($x = 0 - 2$), and detected by nitrate CIMS as clusters with NO_3^-, i.e.,

178   $HOM \cdot NO_3^-$ (Hyttinen et al., 2015). In addition, HOMs' signals were corrected with relative

179   transmission efficiencies of our nitrate CIMS obtained via a method reported previously

180   (Heinritzi et al., 2016).

181   Vocus PTR was applied to quantify precursor concentrations and measure volatile and

182   intermediate volatility oxidation products. The focusing ion-molecule reactor (FIMR) was

183   heated up and its temperature was maintained at 100 °C during the experiments. The FIMR can

184   be operated under 2.0 mbar without a strong interference from corresponding water clusters

185   when ionizing the neutral compounds. The Vocus front and back voltages were 650 V and 15

186   V, respectively, forming an axial voltage of 635V and a reduced electrical field (*E/N*, where E

187   is the electric field strength and N is the number density of the buffer gas in FIMR) of 180 Td.

188   The radio frequency (RF) voltages and frequency were set to be 450 V and 1.3 MHz,

189   respectively. The sample flow was introduced to the Vocus PTR through a Teflon tube with an

190   OD of 1/4 in. and a length of 120 cm from the OFR. A total sample flow of 1.4 slpm was

191   maintained by a pump with an orifice to minimize the delay time of sampling, from which

192   approximately 125 sccm was sampled into the FIMR through a capillary tube.

193   We did not quantify HOMs' concentrations. Since the inner diameters of PAM OFR,

194   sampling tube, and the nitrate CIMS inlet were different, and two reducing unions were used

195   during sampling, the estimation of the penetration efficiency and sampling efficiency of HOMs

196   are of a significant uncertainty. To precisely illustrate changes in the abundance of HOMs at

197   different OH exposures, a normalized signal was chosen to present the abundance of detected

198   HOMs, which is defined as the ratio of the signals of HOMs in the nitrate CIMS normalized by

199   the reagent ions and the initial signal of 1,3,5-TMB, i.e., $S(HOMs)/S(TMB)$. $S(HOMs)$ is the

200   signal of HOM detected by the nitrate CIMS normalized with the signal of reagent ions,

201   whereas $S(TMB)$ is the initial signal of 1,3,5-TMB detected by the Vocus PTR.

202   To further explore the secondary chemistry in the formation and evolution of HOMs, a

203   nominal relative molar yield of HOMs, defined as $S(HOMs)/k[VOCs][OH]$, was used as a

204   substitute of molar HOM yields to reveal their changes under different OH exposures, which is

205   similar to the definition from a previous study (Garmash et al., 2020). k, $[VOCs]$, and $[OH]$

206   stand for the loss coefficient of HOMs in the OFR timing the calibration factor of the nitrate

207   CIMS and then divided by the OH oxidation reaction coefficient of 1,3,5-TMB, 1,3,5-TMB

208   concentration detected at the exit of OFR, and calculated OH concentration in the OFR,

209   respectively. The detailed derivation processes and calculation methods are provided in

210   Supplementary Text S1.

211

3 Results and discussion

A total of 33 HOM monomers with formulae of $C_{7-9}H_{8-16}O_{6-11}$ and 22 HOM dimers with formulae of $C_{17-18}H_{24-30}O_{8-14}$ were observed in the gas phase OH-initiated oxidation of 1,3,5-TMB in the OFR, as listed in Table S2. The relative signal contributions of HOMs to the total signals of all HOMs at an OH exposure of 2.38×10^{10} molecules cm^{-3} s are listed as an example in Table S2. Figure 1 illustrates how OH exposures in the OFR are related to the total normalized signals of HOM monomers and HOM dimers measured at the OFR exit, which is superimposed by a gamma function ($f(x) = ax^m e^{-x}$) simulation line to guide the eyes. The sum of normalized HOM monomers' abundance increased monotonically up to the highest OH exposure of 5×10^{10} molecule cm^{-3} s, whereas those of HOM dimers showed a non-monotonic dependence on OH exposure. The observed faster increase of accretion products than that of HOM monomers can be explained jointly by the fast second-order kinetics for accretion reactions of RO_2(Berndt et al., 2018b) and the high concentrations of relevant radicals in this work. On the other hand, most of the first-generation HOM dimers formed from accretion reactions contain at least one C=C bond and have more functionalities than HOM monomers, and thus should be more reactive to OH radicals, which, together with a faster deposition loss of dimers, results in a faster consumption of HOM dimers than monomers in the OFR. The faster production and consumption of HOM dimers allowed their concentrations to summit at middle levels of OH exposures.

3.1 HOM monomers in the absence of NO_x

Previous studies indicate that oxidation products derived from the peroxide-bicyclic pathway represent a main fraction of HOMs (Wang et al., 2017; Zaytsev et al., 2019). For 1,3,5-TMB, this pathway, as recommended by Master Chemical Mechanism (MCM), starts from a BPR, $C_9H_{13}O_5\cdot$ (MCM name: TM135BPRO2) (Molteni et al., 2018). Scheme 1 has been proposed to provide a good understanding of this reaction system and the structures of oxidation products. Molteni et al. (2018) suggested that $C_9H_{13}O_7\cdot$, i.e., peroxy radical formed from autooxidation of $C_9H_{13}O_5\cdot$ has two isomers, which are referred as C9H13O7A and C9H13O7B for clarity in this study. The structures of these two isomers have been provided in Scheme 1. Their termination products are nominated according to the name of these two isomers, respectively. A second-step of endo-cyclization is required in the formation of C9H13O7B, which is extremely slow and not competitive as shown in several previous studies using both experimental and theoretical approaches (Wang et al., 2017; Xu et al., 2020). Even if such a second O_2 bridging to a double bond is assumed to be possible, the abundance of C9H13O7B should be significantly smaller than C9H13O7A, because of the much faster reaction rate of H-shift reaction in the reaction route for C9H13O7A. Therefore, the majority of HOM monomers

247   are generated from subsequent reactions of $C_9H_{13}O_5\cdot$ and C9H13O7A, both of which contain

248   one C=C bond in the carbon backbone and thus have a feasible site for OH addition. Meanwhile,

249   the autoxidation reaction rate for C9H13O7A should be significantly smaller than $C_9H_{13}O_5\cdot$, as

250   there is no hydrogen atom in $C_9H_{13}O_7\cdot$ that is able to undergo a hydrogen atom shift at an

251   appreciable rate based on our current understanding. Therefore, the subsequent autoxidation

252   reaction should not be able to generate large amounts of more oxidized RO_2.

253   The monomeric termination products of BPR, shown in Scheme 1, were not detected by

254   nitrate CIMS because of their low oxygen content, whereas those of $C_9H_{13}O_7\cdot$ were all

255   observed clearly, including $C_9H_{12}O_6$, $C_9H_{14}O_6$, and $C_9H_{14}O_7$. Especially, $C_9H_{14}O_7$ was the most

256   abundant one among all of the HOM monomer products. As proved by a previous study, these

257   three species should be typical first-generation stabilized products derived from autoxidation

258   (Wang et al., 2020). Their nominal relative molar yields increased with the OH exposures in

259   the OFR, as shown in Figure S1, which implies that the secondary OH reactions of stabilized

260   products can also produce these HOM monomers otherwise the observed yields would remain

261   constant or decline (, the latter of which is due to the consumption of the products). These HOM

262   monomers thus should consist of several isomers bearing the same formula, because products

263   from the secondary reactions cannot share the same structure as that of the one from the first-

264   generation reaction.

265   In addition to these three ones, the nominal relative molar yields of other HOM monomers

266   also showed an increase trend with more OH exposures. The next most prominent products to

267    $C_9H_{14}O_7$ were $C_9H_{16}O_7$ and $C_9H_{16}O_8$ (Figure 2a), which are produced from multi-generation

268   oxidation according to their hydrogen content (Cheng et al., 2021; Molteni et al., 2018). Based

269   on the formulae of these three HOM monomers, they ($C_9H_{14}O_7$, $C_9H_{16}O_7$, and $C_9H_{16}O_8$) could

270   be formed from the bimolecular termination reactions of $C_9H_{15}O_8\cdot$, which can be generated by

271   an OH attack to $C_9H_{14}O_5$, the hydroperoxyl termination product of the BPR $C_9H_{13}O_5\cdot$. The other

272   HOM monomers characterized with high signals were $C_9H_{14}O_8$ and $C_9H_{16}O_9$ (Fig. 2b). These

273   two HOM monomers ($C_9H_{14}O_8$ and $C_9H_{16}O_9$), together with $C_9H_{16}O_8$, correspond to the

274   monomeric termination products of $C_9H_{15}O_9\cdot$, which is highly likely the proxy radical

275   generated by an OH attack to $C_9H_{14}O_6$, i.e., the hydroxyl termination product of $C_9H_{13}O_7\cdot$. As

276   discussed earlier, $C_9H_{13}O_7\cdot$ is a typical autoxidation reaction product of the BPR of $C_9H_{13}O_5\cdot$.

277   Therefore, detected signals of $C_9H_{16}O_8$ should be the sum of two isomers' signals at least. Other

278   HOM monomers were generally observed at much lower signals and thus were not plotted

279   individually.

280   We further examined the nominal relative molar yields of HOM products with 12, 14, and

281   16 hydrogen atoms, i.e., the common HOM monomers in our system. Based on the number of

282 hydrogen atoms, $C_9H_{12}O_m$ (m refers to the oxygen atom number in a molecule) are presumably

283 derived from first generation radicals of $C_9H_{13}O_m\bullet$, and $C_9H_{16}O_m$ are from second generation

284 radicals of $C_9H_{15}O_m\bullet$, whereas $C_9H_{14}O_m$ can be either products of the first-generation or second-

285 generation OH oxidation (Molteni et al., 2018). Therefore, compounds with more hydrogen

286 atoms are expected to increase more rapidly. However, the actual observation in our laboratory

287 experiments conflicted with our preconceived expectations. The nominal relative molar yields

288 of HOM monomers are shown in Figure 3. For clarity, only the 3 most abundant species with

289 (a) 12, (b) 14, and (c) 16 hydrogen atoms, respectively are plotted. A prominent linear increase

290 in the nominal molar yields of $C_9H_{14}O_m$ with larger oxygen atom numbers and $C_9H_{16}O_m$ was

291 observed with the increase of OH exposure, whereas $C_9H_{14}O_m$ with fewer oxygen atoms and

292 $C_9H_{12}O_m$ increased convexly. This is likely because the concentrations of RO_2 in the OFR

293 increased with the increment of consumed precursors, which promoted the carbonyl and

294 hydroxyl channels and favored formation of $C_9H_{12}O_m$ and $C_9H_{14}O_m$ with fewer oxygen atoms

295 in the molecule.

296 It is worth noting that HOM monomers with 18 hydrogen atoms were never observed in

297 our experiments, including a potential stabilized hydroperoxyl products formed from $C_9H_{17}O_m\bullet$.

298 This is expected, since $C_9H_{17}O_m\bullet$ should be in really low concentrations, if ever existed. As

299 indicated by its hydrogen number, a $C_9H_{17}O_m\bullet$ was formed by at least two OH additions to the

300 C=C bond of a $C_9H_{13}O_m\bullet$, but the main BPR, $C_9H_{13}O_5\bullet$, and its autoxidation product ($C_9H_{13}O_7\bullet$),

301 are characterized with one C=C bond on the ring, which makes this formation pathway

302 impossible. Other ring-breakage pathways should not contribute to the formation of this radical

303 ($C_9H_{17}O_m\bullet$) because of their low branching ratio as determined by recent studies (Xu et al., 2020;

304 Zaytsev et al., 2019).

305

306 3.2 HOM dimers in the absence of NO_x

307 Accretion reaction $RO_2 + RO'_2 \rightarrow ROOR' + O_2$ is a source of gas-phase dimer

308 compounds from highly oxidized, functional RO_2 radicals.(Berndt et al., 2018b, 2018a; Ehn et

309 al., 2014; Zhao et al., 2018) $C_{18}H_{26}O_8$ and $C_{18}H_{26}O_{10}$ are two typical accretion reaction products

310 in the 1,3,5-TMB + OH system, whose formation pathways have been elucidated.(Berndt et al.,

311 2018b) $C_{18}H_{26}O_8$ can only be formed via the accretion reaction of two $C_9H_{13}O_5\bullet$. In contrast,

312 $C_{18}H_{26}O_{10}$ can be formed either by the accretion reaction between $C_9H_{13}O_5\bullet$ and $C_9H_{13}O_7\bullet$ or via

313 a second OH attack to $C_{18}H_{26}O_8$. These two HOM dimers are so far the only ones that are

314 confirmed to be formed via the accretion reactions (Berndt et al., 2018b; Bianchi et al., 2019).

315 There are currently no evidences supporting that $C_9H_{15}O_m\bullet$ radicals can participate in the

316 formation of HOM dimers with 28 hydrogens. Therefore, it hints that one could attribute the

317 formation of $C_{18}H_{28}O_m$ to multi-generation OH oxidation of $C_{18}H_{26}O_m$.

318     $C_{18}H_{26}O_{10}$ was characterized with the highest dimer signals for experiments with OH

319 exposures under 3.5×10^{10} molecule cm^{-3} s. Nevertheless, $C_{18}H_{26}O_{10}$, together with $C_{18}H_{28}O_{12}$,

320 $C_{18}H_{26}O_{12}$, $C_{18}H_{28}O_{11}$, $C_{18}H_{28}O_{13}$, and $C_{18}H_{28}O_{10}$ contributed more than 50% of total HOM

321 dimer signals at any OH exposure levels (Fig. S2). These six most abundant HOM dimers

322 correspond exactly to the hydroperoxyl, hydroxyl, and carbonyl termination products of

323 $C_{18}H_{27}O_{11}\cdot$ and $C_{18}H_{27}O_{13}\cdot$, respectively. These two RO_2 ($C_{18}H_{27}O_{11}\cdot$ and $C_{18}H_{27}O_{13}\cdot$), on the

324 other hand, could be generated by OH attacks to $C_{18}H_{26}O_8$ and $C_{18}H_{26}O_{10}$, respectively, which

325 strongly suggests the significant role of secondary OH chemistry in the formation of HOMs in

326 our experiments. Figure 4 shows the normalized signals of these abundant HOM dimers at

327 different OH exposures. These HOM dimers increased under low OH exposure levels but

328 decreased with the increasing OH exposure that corresponds to 2.8 – 6.9 hours' atmospheric

329 equivalent photochemical age.

330   The nominal relative molar yields of the abovementioned HOM dimers are shown in

331 Figure 5 as a function of OH exposure, except for $C_{18}H_{28}O_{11}$. The nominal relative molar yields

332 of $C_{18}H_{28}O_{11}$ are not plotted in the Figure 5, since they overlapped quite closely with those of

333 $C_{18}H_{26}O_{10}$, as can be deduced from Figure 4b. Compared with HOM monomers, variation

334 tendencies of the nominal relative molar yields of HOM dimers are more diverse. Especially,

335 the nominal relative molar yield of $C_{18}H_{26}O_8$ (Fig. S3) kept declination under growing OH

336 exposure conditions, whereas that of $C_{18}H_{26}O_{10}$ (Fig. 5) appeared to reduce after a slight growth

337 in the OH exposure range studied. The changes in the nominal relative molar yields of these

338 two HOM dimers along with the OH exposure confirm the combined influences of accretion

339 reactions and multi-generation OH oxidation reactions on their formation and evolution, i.e.,

340 further OH oxidation consumed $C_{18}H_{26}O_8$ and $C_{18}H_{26}O_{10}$, and produced $C_{18}H_{26}O_{10}$, $C_{18}H_{26}O_{12}$,

341 $C_{18}H_{28}O_{10}$, $C_{18}H_{28}O_{11}$, $C_{18}H_{28}O_{12}$ and $C_{18}H_{28}O_{13}$. These six HOM dimers contributed the

342 majority of the total HOM dimer signals as mentioned above, while most of them were HOM

343 dimers with 28 hydrogen atoms.

344   The nominal relative molar yields of dimer compounds with 28 hydrogen atoms tended to

345 increase with extended OH exposures, except that $C_{18}H_{28}O_{10}$ appeared to keep constant when

346 OH exposure was larger than 1×10^{10} molecules cm^{-3} s. This again indicates that these H28

347 products might be formed by an OH addition to a C=C bond in the accretion products, and then

348 the newly formed alkyl radical further reacted and would go through the typical RO_2

349 termination reactions.

350   It should be noted that the gas-phase chemistry in the PAM OFR cannot be exactly the
351   same as that in the ambient. Reactions of OH with OVOCs often lead to HO_2 formation,
352   resulting in a HO_2:RO_2 ratio larger than 1 in the real atmosphere (Bianchi et al., 2019). A recent
353   campaign conducted at a rural site in the Yangtze River Delta estimated that the local ratio of
354   HO_2:RO_2, the latter of which was presumably derived from longer chain alkanes ($> C_3$), alkenes,
355   and aromatic compounds, was around 1.66 (Ma et al., 2022). Such a high OH:HO_2 ratio
356   condition is typically difficult to be simulated in the laboratory experiments, as the precursors
357   are usually hydrocarbons without any OVOCs (Peng and Jimenez, 2020). This is exactly the
358   case for our experiments and the lower ratio of OH:HO_2 in our experiments than that in the
359   ambient atmosphere was confirmed by a photochemical model in our previous study (Wang et
360   al., 2020). In addition, high concentrations of radicals might also terminate the RO_2 chain earlier,
361   which inhibits the autoxidation reactions in the PAM OFR. However, these could only
362   influence the distribution of oxidation products at most, and would not affect the chemical
363   behaviors of HOMs under different OH exposures.

364   Such an active secondary OH chemistry is consistent with the fast OH reaction rates of
365   HOMs. We take $C_{18}H_{26}O_8$ as an example, which is the accretion product of two $C_9H_{13}O_5$·. Its
366   OH reaction rate constant is estimated to be around 2.07×10^{-10} cm^3 molecule^{-1} s^{-1} according to
367   the structure-activity relationship (Jenkin et al., 2018b, 2018a), whose details are provided in
368   Supplementary Text S2. This rate is several times larger than that of 1,3,5-TMB, which enables
369   a very active secondary OH chemistry in the system. MCM recommended an OH reaction rate
370   of 1.28×10^{-10} cm^3 molecule^{-1} s^{-1} for TM135BPOOH ($C_9H_{14}O_5$) and 1.00×10^{-10} cm^3 molecule^{-1}
371   s^{-1} for TM135OBPOH ($C_9H_{12}O_4$) (Jenkin et al., 2003). The OH reaction rate for $C_{18}H_{26}O_8$
372   should be around twice of these values, as there are two C=C bonds in its structure. Our
373   calculation result is consistent with this estimation.

374

375   3.3 Products in the presence of NO_x

376   Scheme 2 shows the NO termination pathways of the main BPR $C_9H_{13}O_5$· and its
377   autoxidation product, $C_9H_{13}O_7$·. After introducing N_2O into PAM OFR, quantities of
378   organonitrates were generated, including both C9 and C18 organonitrates. The averaged mass
379   spectrometry of nitrate CIMS in the 1.8 ppb NO experiment and 4.8 ppb NO experiment is
380   shown in Figure S4. Organonitrates were formed via the NO + RO_2 reaction, called as NO
381   termination reactions. The distribution of oxidation products under these two NO settings were
382   similar.

383   As discussed above, most of the first-generation HOMs should contain a C=C bond in the
384   carbon backbone. The ubiquitous existence of organonitrates that contain two nitrogen atoms

385   exactly confirms the extensive secondary OH oxidation in the systems, because the NO

386   termination reaction of RO_2 is the only pathway that can generate organonitrates and this

387   pathway can only introduce one nitrogen atom at a time, as indicated in Scheme 2. Taking the

388   most abundant organonitrate, $C_9H_{14}N_2O_{10}$, as an example, it was exactly the NO termination

389   product of $C_9H_{14}NO_9\cdot$, which was generated from an OH attack and a subsequent O_2 addition

390   to $C_9H_{13}NO_6$, the NO termination product of $C_9H_{13}O_5\cdot$. For other organonitrates, $C_9H_{13}NO_8$, the

391   second most abundant organonitrate, could be either a NO termination product of $C_9H_{13}O_7\cdot$ or,

392   together with other most abundant organonitrates, $C_9H_{15}NO_7$ and $C_9H_{15}NO_8$, classical

393   termination products of $C_9H_{14}NO_9\cdot$.

394   The distributions of C18 organonitrates also verified the extensive secondary reactions.

395   The most abundant C18 organonitrate, $C_{18}H_{27}NO_{12}$ was a NO termination product of radical

396    $C_{18}H_{27}O_{11}\cdot$, which, as mentioned above, was the radical generated from the OH reaction with

397    $C_{18}H_{26}O_8$. Other C18 organonitrates are believed to be formed in a similar pathway since no

398   evidence supports that a nitrogen-containing monomeric RO_2 can go through accretion

399   reactions. Hence, plenty of organonitrates have been formed via the multi-generation OH

400   reactions of first-generation stabilized products.

401

402   **4 Atmospheric Implications**

403   This study highlights the influences of OH exposure on the distribution and evolution of

404   1,3,5-TMB-derived HOMs. Secondary OH reactions can influence HOMs' composition by

405   directly reacting with the stabilized first-generation oxidation products, leading to enhanced

406   formation of HOMs. Organonitrates generated in the NO experiments further confirmed this.

407   Due to the elevated abundance and the reduced volatility of HOMs, growth rates of newly

408   formed nanoparticles in the presence of HOMs should be raised, especially in high-OH

409   environments, which prevails in the summer noon. Substantially high concentrations of OH

410   have been frequently observed in polluted environments during summer, e.g., megacities in

411   China (Tan et al., 2019), and thus more active secondary OH reactions are expected compared

412   to wintertime. As a plausible consequence, seasonal differences of HOMs and new particle

413   formation (NPF) are resulted (Guo et al., 2022; Qiao et al., 2021; Yao et al., 2018). Furthermore,

414   previous studies suggest that high concentrations of NO can suppress the formation of HOMs

415   via the suppression of autoxidation (Pye et al., 2019), but the influences of such a suppression

416   could have been overestimated, since secondary OH reactions can continue to oxidize the

417   stabilized organonitrates. Our conclusions help to explain the existing gap between model

418   prediction and ambient measurement on the HOMs concentrations (Qi et al., 2018), and to build

419   a global HOMs simulation model.

420

421 *Data availability.* Data used in this work are available upon request from the corresponding
422 authors.

423

424 *Supplement.* The supplement related to this article is available online.

425

426 *Author contributions.* LW and Yuwei Wang designed the experiments. Yuwei Wang conducted
427 the laboratory experiments. Yuwei Wang analyzed the data. Yuwei Wang and LW wrote the
428 paper. All co-authors discussed the results and commented on the manuscript.

429

430 *Competing interests.* The authors declare that they have no conflict of interest.

431

References

434 **References**

435 Berndt, T., Mentler, B., Scholz, W., Fischer, L., Herrmann, H., Kulmala, M. and Hansel, A.:
436 Accretion Product Formation from Ozonolysis and OH Radical Reaction of α-Pinene:
437 Mechanistic Insight and the Influence of Isoprene and Ethylene, Environ. Sci. Technol.,
438 52(19), 11069–11077, doi:10.1021/acs.est.8b02210, 2018a.

439 Berndt, T., Scholz, W., Mentler, B., Fischer, L., Herrmann, H., Kulmala, M. and Hansel, A.:
440 Accretion Product Formation from Self- and Cross-Reactions of RO2 Radicals in the
441 Atmosphere, Angew. Chemie - Int. Ed., 57(14), 3820–3824, doi:10.1002/anie.201710989,
442 2018b.

443 Bianchi, F., Kurtén, T., Riva, M., Mohr, C., Rissanen, M. P., Roldin, P., Berndt, T., Crounse,
444 J. D., Wennberg, P. O., Mentel, T. F., Wildt, J., Junninen, H., Jokinen, T., Kulmala, M.,
445 Worsnop, D. R., Thornton, J. A., Donahue, N., Kjaergaard, H. G. and Ehn, M.: Highly
446 Oxygenated Organic Molecules (HOM) from Gas-Phase Autoxidation Involving Peroxy
447 Radicals: A Key Contributor to Atmospheric Aerosol, Chem. Rev., 119(6), 3472–3509,
448 doi:10.1021/acs.chemrev.8b00395, 2019.

449 Cheng, X., Chen, Q., Li, Y. J., Zheng, Y., Liao, K. and Huang, G.: Highly Oxygenated
450 Organic Molecules Produced by the Oxidation of Benzene and Toluene in a Wide Range of
451 OH Exposure and NOx Conditions, Atmos. Chem. Phys., (x), 1–23, doi:10.5194/acp-2021-
452 201, 2021.

453 Crounse, J. D., Nielsen, L. B., Jørgensen, S., Kjaergaard, H. G. and Wennberg, P. O.:
454 Autoxidation of organic compounds in the atmosphere, J. Phys. Chem. Lett., 4(20), 3513–
455 3520, doi:10.1021/jz4019207, 2013.

456 Ehn, M., Thornton, J. A., Kleist, E., Sipilä, M., Junninen, H., Pullinen, I., Springer, M.,
457 Rubach, F., Tillmann, R., Lee, B., Lopez-Hilfiker, F., Andres, S., Acir, I. H., Rissanen, M.,
458 Jokinen, T., Schobesberger, S., Kangasluoma, J., Kontkanen, J., Nieminen, T., Kurtén, T.,
459 Nielsen, L. B., Jørgensen, S., Kjaergaard, H. G., Canagaratna, M., Maso, M. D., Berndt, T.,
460 Petäjä, T., Wahner, A., Kerminen, V. M., Kulmala, M., Worsnop, D. R., Wildt, J. and Mentel,
461 T. F.: A large source of low-volatility secondary organic aerosol, Nature, 506(7489), 476–
462 479, doi:10.1038/nature13032, 2014.

463 Eisele, F. L. and Tanner, D. J.: Measurement of the gas phase concentration of H 2 SO 4 and
464 methane sulfonic acid and estimates of H 2 SO 4 production and loss in the atmosphere, J.
465 Geophys. Res. Atmos., 98(D5), 9001–9010, doi:10.1029/93JD00031, 1993.

466 Garmash, O., Rissanen, M. P., Pullinen, I., Schmitt, S., Kausiala, O., Tillmann, R., Zhao, D.,
467 Percival, C., Bannan, T. J., Priestley, M., Hallquist, Å. M., Kleist, E., Kiendler-Scharr, A.,
468 Hallquist, M., Berndt, T., McFiggans, G., Wildt, J., Mentel, T. F. and Ehn, M.: Multi-
469 generation OH oxidation as a source for highly oxygenated organic molecules from
470 aromatics, Atmos. Chem. Phys., 20(1), 515–537, doi:10.5194/acp-20-515-2020, 2020.

471 Guo, Y., Yan, C., Liu, Y., Qiao, X., Zheng, F., Zhang, Y., Zhou, Y., Li, C., Fan, X., Lin, Z.,
472 Feng, Z., Zhang, Y., Zheng, P., Tian, L., Nie, W., Wang, Z., Huang, D., Daellenbach, K. R.,
473 Yao, L., Dada, L., Bianchi, F., Jiang, J., Liu, Y., Kerminen, V. M. and Kulmala, M.: Seasonal
474 variation in oxygenated organic molecules in urban Beijing and their contribution to
475 secondary organic aerosol, Atmos. Chem. Phys., 22(15), 10077–10097, doi:10.5194/acp-22-
476 10077-2022, 2022.

477 Heinritzi, M., Simon, M., Steiner, G., Wagner, A. C., Kürten, A., Hansel, A. and Curtius, J.:
478 Characterization of the mass-dependent transmission efficiency of a CIMS, Atmos. Meas.
479 Tech., 9(4), 1449–1460, doi:10.5194/amt-9-1449-2016, 2016.
480 Hyttinen, N., Kupiainen-Määttä, O., Rissanen, M. P., Muuronen, M., Ehn, M. and Kurtén, T.:
481 Modeling the Charging of Highly Oxidized Cyclohexene Ozonolysis Products Using Nitrate-
482 Based Chemical Ionization, J. Phys. Chem. A, 119(24), 6339–6345,
483 doi:10.1021/acs.jpca.5b01818, 2015.
484 Jenkin, M. E., Saunders, S. M., Wagner, V. and Pilling, M. J.: Protocol for the development
485 of the Master Chemical Mechanism, MCM v3 (Part B): tropospheric degradation of aromatic
486 volatile organic compounds, Atmos. Chem. Phys., 3(1), 181–193, doi:10.5194/acp-3-181-
487 2003, 2003.
488 Jenkin, M. E., Valorso, R., Aumont, B., Rickard, A. R. and Wallington, T. J.: Estimation of
489 rate coefficients and branching ratios for gas-phase reactions of OH with aliphatic organic
490 compounds for use in automated mechanism construction., 2018a.
491 Jenkin, M. E., Valorso, R., Aumont, B., Rickard, A. R. and Wallington, T. J.: Estimation of
492 rate coefficients and branching ratios for gas-phase reactions of OH with aromatic organic
493 compounds for use in automated mechanism construction, Atmos. Chem. Phys., 18(13),
494 9329–9349, doi:10.5194/acp-18-9329-2018, 2018b.
495 Krechmer, J., Lopez-Hilfiker, F., Koss, A., Hutterli, M., Stoermer, C., Deming, B., Kimmel,
496 J., Warneke, C., Holzinger, R., Jayne, J., Worsnop, D., Fuhrer, K., Gonin, M. and De Gouw,
497 J.: Evaluation of a New Reagent-Ion Source and Focusing Ion− Molecule Reactor for Use in
498 Proton-Transfer-Reaction Mass Spectrometry, Anal. Chem., 90, 12011–12018,
499 doi:10.1021/acs.analchem.8b02641, 2018.
500 Lambe, A. T., Ahern, A. T., Williams, L. R., Slowik, J. G., Wong, J. P. S., Abbatt, J. P. D.,
501 Brune, W. H., Ng, N. L., Wright, J. P., Croasdale, D. R., Worsnop, D. R., Davidovits, P. and
502 Onasch, T. B.: Characterization of aerosol photooxidation flow reactors: heterogeneous
503 oxidation, secondary organic aerosol formation and cloud condensation nuclei activity
504 measurements, Atmos. Meas. Tech, 4, 445–461, doi:10.5194/amt-4-445-2011, 2011.
505 Lambe, A. T., Chhabra, P. S., Onasch, T. B., Brune, W. H., Hunter, J. F., Kroll, J. H.,
506 Cummings, M. J., Brogan, J. F., Parmar, Y., Worsnop, D. R., Kolb, C. E. and Davidovits, P.:
507 Effect of oxidant concentration, exposure time, and seed particles on secondary organic
508 aerosol chemical composition and yield, Atmos. Chem. Phys., 15(6), 3063–3075,
509 doi:10.5194/acp-15-3063-2015, 2015.
510 Lehtipalo, K., Yan, C., Dada, L., Bianchi, F., Xiao, M., Wagner, R., Stolzenburg, D., Ahonen,
511 L. R., Amorim, A., Baccarini, A., Bauer, P. S., Baumgartner, B., Bergen, A., Bernhammer, A.
512 K., Breitenlechner, M., Brilke, S., Buchholz, A., Mazon, S. B., Chen, D., Chen, X., Dias, A.,
513 Dommen, J., Draper, D. C., Duplissy, J., Ehn, M., Finkenzeller, H., Fischer, L., Frege, C.,
514 Fuchs, C., Garmash, O., Gordon, H., Hakala, J., He, X., Heikkinen, L., Heinritzi, M., Helm, J.
515 C., Hofbauer, V., Hoyle, C. R., Jokinen, T., Kangasluoma, J., Kerminen, V. M., Kim, C.,
516 Kirkby, J., Kontkanen, J., Kürten, A., Lawler, M. J., Mai, H., Mathot, S., Mauldin, R. L.,
517 Molteni, U., Nichman, L., Nie, W., Nieminen, T., Ojdanic, A., Onnela, A., Passananti, M.,
518 Petäjä, T., Piel, F., Pospisilova, V., Quéléver, L. L. J., Rissanen, M. P., Rose, C., Sarnela, N.,
519 Schallhart, S., Schuchmann, S., Sengupta, K., Simon, M., Sipilä, M., Tauber, C., Tomé, A.,
520 Tröstl, J., Väisänen, O., Vogel, A. L., Volkamer, R., Wagner, A. C., Wang, M., Weitz, L.,

521   Wimmer, D., Ye, P., Ylisirniö, A., Zha, Q., Carslaw, K. S., Curtius, J., Donahue, N. M.,
522   Flagan, R. C., Hansel, A., Riipinen, I., Virtanen, A., Winkler, P. M., Baltensperger, U.,
523   Kulmala, M. and Worsnop, D. R.: Multicomponent new particle formation from sulfuric acid,
524   ammonia, and biogenic vapors, Sci. Adv., 4(12), 1–10, doi:10.1126/sciadv.aau5363, 2018.
525   Lu, K. D., Rohrer, F., Holland, F., Fuchs, H., Bohn, B., Brauers, T., Chang, C. C., Häseler, R.,
526   Hu, M., Kita, K., Kondo, Y., Li, X., Lou, S. R., Nehr, S., Shao, M., Zeng, L. M., Wahner, A.,
527   Zhang, Y. H. and Hofzumahaus, A.: Observation and modelling of OH and HO2
528   concentrations in the Pearl River Delta 2006: A missing OH source in a VOC rich
529   atmosphere, Atmos. Chem. Phys., 12(3), 1541–1569, doi:10.5194/acp-12-1541-2012, 2012.
530   Ma, X., Tan, Z., Lu, K., Yang, X., Chen, X., Wang, H., Chen, S., Fang, X., Li, S., Li, X., Liu,
531   J., Liu, Y., Lou, S., Qiu, W., Wang, H., Zeng, L. and Zhang, Y.: OH and HO2 radical
532   chemistry at a suburban site during the EXPLORE-YRD campaign in 2018, Atmos. Chem.
533   Phys., 22(10), 7005–7028, doi:10.5194/acp-22-7005-2022, 2022.
534   Mentel, T. F., Springer, M., Ehn, M., Kleist, E., Pullinen, I., Kurtén, T., Rissanen, M.,
535   Wahner, A. and Wildt, J.: Formation of highly oxidized multifunctional compounds:
536   Autoxidation of peroxy radicals formed in the ozonolysis of alkenes - Deduced from
537   structure-product relationships, Atmos. Chem. Phys., 15(12), 6745–6765, doi:10.5194/acp-
538   15-6745-2015, 2015.
539   Mohr, C., Thornton, J. A., Heitto, A., Lopez-hil, F. D., Lutz, A., Riipinen, I., Hong, J.,
540   Donahue, N. M., Hallquist, M., Petäjä, T., Kulmala, M. and Yli-juuti, T.: Molecular
541   identification of organic vapors driving atmospheric nanoparticle growth, Nat. Commun.,
542   (2019), 1–7, doi:10.1038/s41467-019-12473-2, 2019.
543   Molteni, U., Bianchi, F., Klein, F., Haddad, I. El, Frege, C., Rossi, M. J., Dommen, J. and
544   Baltensperger, U.: Formation of highly oxygenated organic molecules from aromatic
545   compounds, Atmos. Chem. Phys, 18, 1909–1921, doi:10.5194/acp-18-1909-2018, 2018.
546   Ng, N. L., Canagaratna, M. R., Zhang, Q., Jimenez, J. L., Tian, J., Ulbrich, I. M., Kroll, J. H.,
547   Docherty, K. S., Chhabra, P. S., Bahreini, R., Murphy, S. M., Seinfeld, J. H., Hildebrandt, L.,
548   Donahue, N. M., Decarlo, P. F., Lanz, V. A., Prévôt, A. S. H., Dinar, E., Rudich, Y. and
549   Worsnop, D. R.: Organic aerosol components observed in Northern Hemispheric datasets
550   from Aerosol Mass Spectrometry, Atmos. Chem. Phys., 10(10), 4625–4641, doi:10.5194/acp-
551   10-4625-2010, 2010.
552   Otkjær, R. V., Jakobsen, H. H., Tram, C. M. and Kjaergaard, H. G.: Calculated Hydrogen
553   Shift Rate Constants in Substituted Alkyl Peroxy Radicals, J. Phys. Chem. A, 122(43), 8665–
554   8673, doi:10.1021/acs.jpca.8b06223, 2018.
555   Peng, Z. and Jimenez, J. L.: Radical chemistry in oxidation flow reactors for atmospheric
556   chemistry research, Chem. Soc. Rev., 49(9), 2570–2616, doi:10.1039/c9cs00766k, 2020.
557   Pye, H. O. T., D'Ambro, E. L., Lee, B. H., Schobesberger, S., Takeuchi, M., Zhao, Y., Lopez-
558   Hilfiker, F., Liu, J., Shilling, J. E., Xing, J., Mathur, R., Middlebrook, A. M., Liao, J., Welti,
559   A., Graus, M., Warneke, C., de Gouw, J. A., Holloway, J. S., Ryerson, T. B., Pollack, I. B.
560   and Thornton, J. A.: Anthropogenic enhancements to production of highly oxygenated
561   molecules from autoxidation, Proc. Natl. Acad. Sci. U. S. A., 116(14), 6641–6646,
562   doi:10.1073/pnas.1810774116, 2019.
563   Qi, X., Ding, A., Roldin, P., Xu, Z., Zhou, P., Sarnela, N., Nie, W., Huang, X., Rusanen, A.,
564   Ehn, M., Rissanen, M. P., Petäjä, T., Kulmala, M. and Boy, M.: Modelling studies of HOMs

565   and their contributions to new particle formation and growth: comparison of boreal forest in
566   Finland and a polluted environment in China, Atmos. Chem. Phys, 18, 11779–11791,
567   doi:10.5194/acp-18-11779-2018, 2018.
568   Qiao, X., Yan, C., Li, X., Guo, Y., Yin, R., Deng, C., Li, C., Nie, W., Wang, M., Cai, R.,
569   Huang, D., Wang, Z., Yao, L., Worsnop, D. R., Bianchi, F., Liu, Y., Donahue, N. M.,
570   Kulmala, M. and Jiang, J.: Contribution of Atmospheric Oxygenated Organic Compounds to
571   Particle Growth in an Urban Environment, Environ. Sci. Technol.,
572   doi:10.1021/acs.est.1c02095, 2021.
573   Qu, H., Wang, Y., Zhang, R., Liu, X., Huey, L. G., Sjostedt, S., Zeng, L., Lu, K., Wu, Y.,
574   Shao, M., Hu, M., Tan, Z., Fuchs, H., Broch, S., Wahner, A., Zhu, T. and Zhang, Y.:
575   Chemical Production of Oxygenated Volatile Organic Compounds Strongly Enhances
576   Boundary-Layer Oxidation Chemistry and Ozone Production, Environ. Sci. Technol., 55(20),
577   13718–13727, doi:10.1021/acs.est.1c04489, 2021.
578   Stolzenburg, D., Fischer, L., Vogel, A. L., Heinritzi, M., Schervish, M., Simon, M., Wagner,
579   A. C., Dada, L., Ahonen, L. R., Amorim, A., Baccarini, A., Bauer, P. S., Baumgartner, B.,
580   Bergen, A., Bianchi, F., Breitenlechner, M., Brilke, S., Mazon, S. B., Chen, D., Dias, A.,
581   Draper, D. C., Duplissy, J., Haddad, I. El, Finkenzeller, H., Frege, C., Fuchs, C., Garmash, O.,
582   Gordon, H., He, X., Helm, J., Hofbauer, V., Hoyle, C. R., Kim, C., Kirkby, J., Kontkanen, J.,
583   Kürten, A., Lampilahti, J., Lawler, M., Lehtipalo, K., Leiminger, M., Mai, H., Mathot, S.,
584   Mentler, B., Molteni, U., Nie, W., Nieminen, T., Nowak, J. B., Ojdanic, A., Onnela, A.,
585   Passananti, M., Petäjä, T., Quéléver, L. L. J., Rissanen, M. P., Sarnela, N., Schallhart, S.,
586   Tauber, C., Tomé, A., Wagner, R., Wang, M., Weitz, L., Wimmer, D., Xiao, M., Yan, C., Ye,
587   P., Zha, Q., Baltensperger, U., Curtius, J., Dommen, J., Flagan, R. C., Kulmala, M., Smith, J.
588   N., Worsnop, D. R., Hansel, A., Donahue, N. M. and Winkler, P. M.: Rapid growth of organic
589   aerosol nanoparticles over a wide tropospheric temperature range, Proc. Natl. Acad. Sci. U. S.
590   A., 115(37), 9122–9127, doi:10.1073/pnas.1807604115, 2018.
591   Tan, Z., Lu, K., Jiang, M., Su, R., Wang, H., Lou, S., Fu, Q., Zhai, C., Tan, Q., Yue, D.,
592   Chen, D., Wang, Z., Xie, S., Zeng, L. and Zhang, Y.: Daytime atmospheric oxidation capacity
593   in four Chinese megacities during the photochemically polluted season: A case study based
594   on box model simulation, Atmos. Chem. Phys., 19(6), 3493–3513, doi:10.5194/acp-19-3493-
595   2019, 2019.
596   Tröstl, J., Chuang, W. K., Gordon, H., Heinritzi, M., Yan, C., Molteni, U., Ahlm, L., Frege,
597   C., Bianchi, F., Wagner, R., Simon, M., Lehtipalo, K., Williamson, C., Craven, J. S.,
598   Duplissy, J., Adamov, A., Almeida, J., Bernhammer, A. K., Breitenlechner, M., Brilke, S.,
599   Dias, A., Ehrhart, S., Flagan, R. C., Franchin, A., Fuchs, C., Guida, R., Gysel, M., Hansel, A.,
600   Hoyle, C. R., Jokinen, T., Junninen, H., Kangasluoma, J., Keskinen, H., Kim, J., Krapf, M.,
601   Kürten, A., Laaksonen, A., Lawler, M., Leiminger, M., Mathot, S., Möhler, O., Nieminen, T.,
602   Onnela, A., Petäjä, T., Piel, F. M., Miettinen, P., Rissanen, M. P., Rondo, L., Sarnela, N.,
603   Schobesberger, S., Sengupta, K., Sipilä, M., Smith, J. N., Steiner, G., Tomè, A., Virtanen, A.,
604   Wagner, A. C., Weingartner, E., Wimmer, D., Winkler, P. M., Ye, P., Carslaw, K. S., Curtius,
605   J., Dommen, J., Kirkby, J., Kulmala, M., Riipinen, I., Worsnop, D. R., Donahue, N. M. and
606   Baltensperger, U.: The role of low-volatility organic compounds in initial particle growth in
607   the atmosphere, Nature, 533(7604), 527–531, doi:10.1038/nature18271, 2016.

608   Tsiligiannis, E., Hammes, J., Salvador, C. M., Mentel, T. F. and Hallquist, M.: Effect of NOx
609   on 1,3,5-trimethylbenzene (TMB) oxidation product distribution and particle formation,
610   Atmos. Chem. Phys., 19(23), 15073–15086, doi:10.5194/acp-19-15073-2019, 2019.
611   Wang, S., Wu, R., Berndt, T., Ehn, M. and Wang, L.: Formation of Highly Oxidized Radicals
612   and Multifunctional Products from the Atmospheric Oxidation of Alkylbenzenes, Environ.
613   Sci. Technol., 51(15), 8442–8449, doi:10.1021/acs.est.7b02374, 2017.
614   Wang, W., Yuan, B., Peng, Y., Su, H., Cheng, Y. and Yang, S.: Direct observations indicate
615   photodegradable oxygenated VOCs as larger contributors to radicals and ozone production in
616   the atmosphere, Atmos. Chem. Phys., (December), 1–28, 2022.
617   Wang, Y., Mehra, A., Krechmer, J. E., Yang, G., Hu, X., Lu, Y., Lambe, A., Canagaratna, M.,
618   Chen, J., Worsnop, D., Coe, H. and Wang, L.: Oxygenated products formed from OH-
619   initiated reactions of trimethylbenzene: autoxidation and accretion, Atmos. Chem. Phys.,
620   20(15), 9563–9579, doi:10.5194/acp-20-9563-2020, 2020.
621   Xu, L., Møller, K. H., Crounse, J. D., Kjaergaard, H. G. and Wennberg, P. O.: New insights
622   into the radical chemistry and product distribution in the OH-initiated oxidation of benzene,
623   Environ. Sci. Technol., 54(21), 13467–13477, doi:10.1021/acs.est.0c04780, 2020.
624   Yao, L., Garmash, O., Bianchi, F., Zheng, J., Yan, C., Kontkanen, J., Junninen, H., Mazon, S.
625   B., Ehn, M., Paasonen, P., Sipilä, M., Wang, M., Wang, X., Xiao, S., Chen, H., Lu, Y.,
626   Zhang, B., Wang, D., Fu, Q., Geng, F., Li, L., Wang, H., Qiao, L., Yang, X., Chen, J.,
627   Kerminen, V.-M., Petäjä, T., Worsnop, D. R., Kulmala, M. and Wang, L.: Atmospheric new
628   particle formation from sulfuric acid and amines in a Chinese megacity, Science (80-.).,
629   361(6399), 278–281, doi:10.1126/science.aao4839, 2018.
630   Yuan, B., Chen, W., Shao, M., Wang, M., Lu, S., Wang, B., Liu, Y., Chang, C. C. and Wang,
631   B.: Measurements of ambient hydrocarbons and carbonyls in the Pearl River Delta (PRD),
632   China, Atmos. Res., 116, 93–104, doi:10.1016/j.atmosres.2012.03.006, 2012.
633   Zaytsev, A., Koss, A. R., Breitenlechner, M., Krechmer, J. E., Nihill, K. J., Lim, C. Y., Rowe,
634   J. C., Cox, J. L., Moss, J., Roscioli, J. R., Canagaratna, M. R., Worsnop, D. R., Kroll, J. H.
635   and Keutsch, F. N.: Mechanistic study of the formation of ring-retaining and ring-opening
636   products from the oxidation of aromatic compounds under urban atmospheric conditions,
637   Atmos. Chem. Phys., 19(23), 15117–15129, doi:10.5194/acp-19-15117-2019, 2019.
638   Zhao, Y., Thornton, J. A. and Pye, H. O. T.: Quantitative constraints on autoxidation and
639   dimer formation from direct probing of monoterpene-derived peroxy radical chemistry, Proc.
640   Natl. Acad. Sci., 115(48), 12142–12147, doi:10.1073/pnas.1812147115, 2018.
641

Figure Captions

Figure 1. Normalized signals of HOM monomers and HOM dimers measured at the exit of OFR in experiments without NOx as a function of OH exposure. The solid lines represent fitting results using a gamma function to guide the eye.

Figure 2. Normalized signals of (a) $C_9H_{14}O_7$, $C_9H_{16}O_7$, and $C_9H_{16}O_8$ and (b) $C_9H_{14}O_8$, $C_9H_{16}O_8$, and $C_9H_{16}O_9$ measured at the exit of OFR in experiments without NO_x as a function of OH exposure. $C_9H_{16}O_8$ are shown in both plots to better illustrate the chemical profiles of different compound groups.

Figure 3. The nominal relative molar yield of HOM monomers containing (a) 12, (b) 14, and (c) 16 hydrogen atoms as a function of OH exposure in the OH-initiated 1,3,5-TMB oxidation experiments.

Figure 4. Normalized signals of (a) $C_{18}H_{26}O_{12}$, $C_{18}H_{28}O_{12}$, and $C_{18}H_{28}O_{13}$, and (b) $C_{18}H_{26}O_{10}$, $C_{18}H_{28}O_{10}$, and $C_{18}H_{28}O_{11}$ measured at the exit of OFR in experiments without NOx as a function of OH exposure.

Figure 5. The nominal relative molar yield of (a) $C_{18}H_{26}O_{10}$ and $C_{18}H_{26}O_{12}$ and (b) $C_{18}H_{28}O_{10}$, $C_{18}H_{28}O_{12}$, and $C_{18}H_{28}O_{13}$ as a function of OH exposure in the OH-initiated 1,3,5-TMB oxidation experiments.
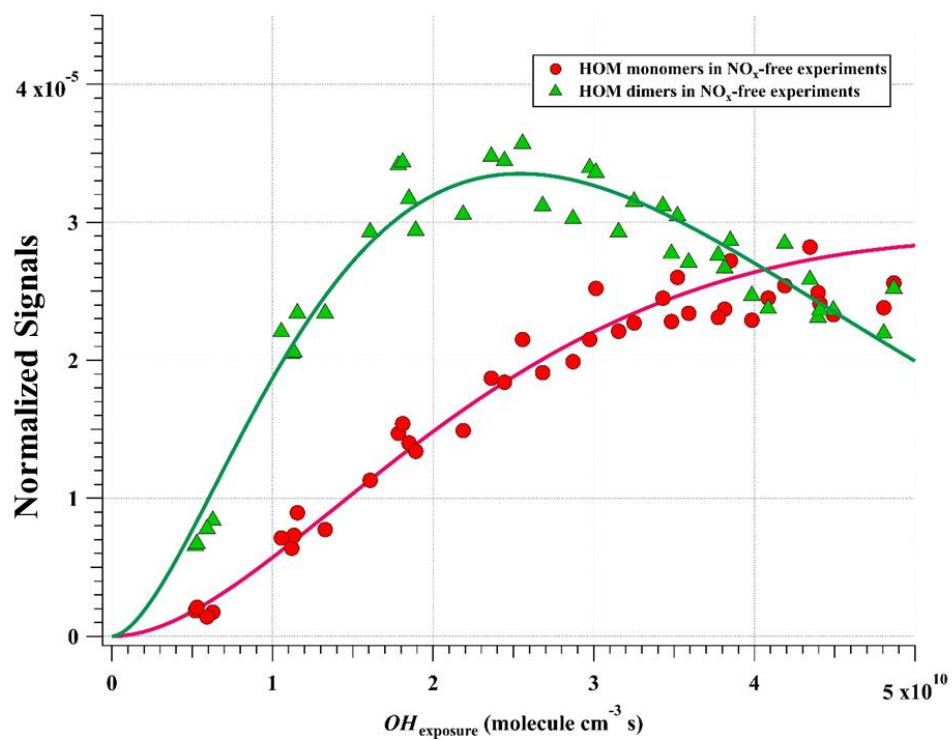
Figure 1
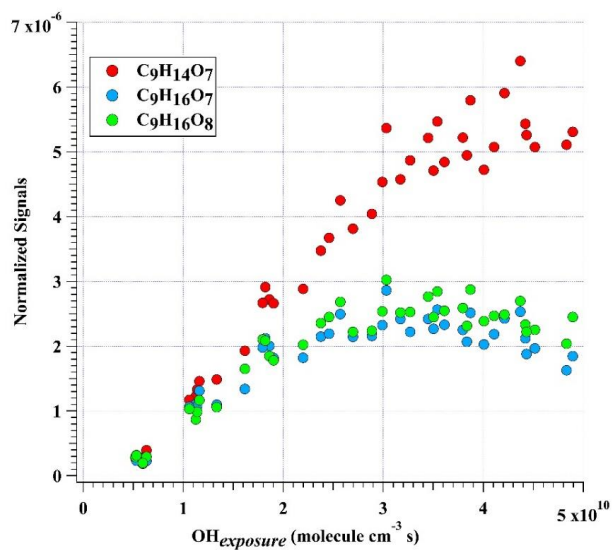
Figure 2a
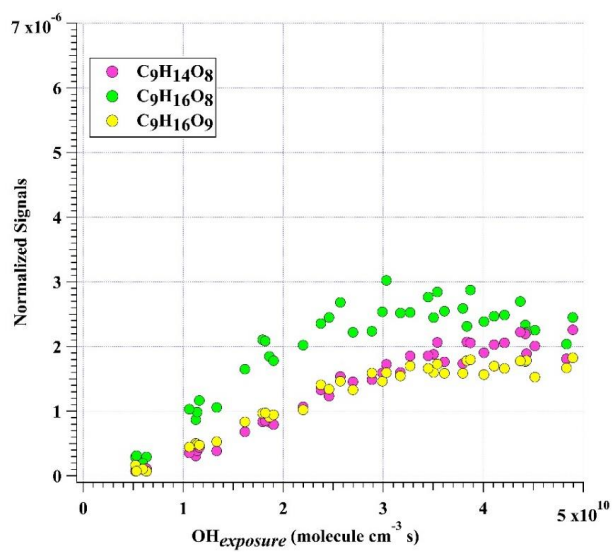
Figure 2b
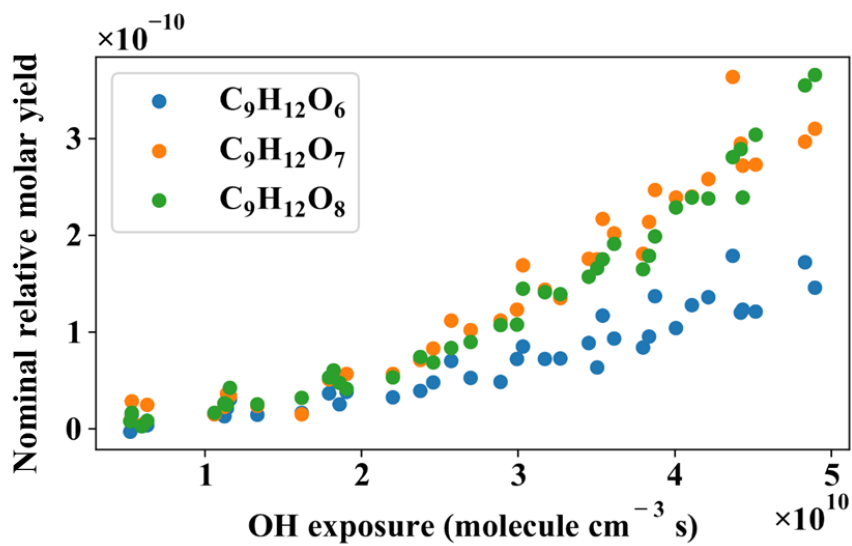
Figure 3a
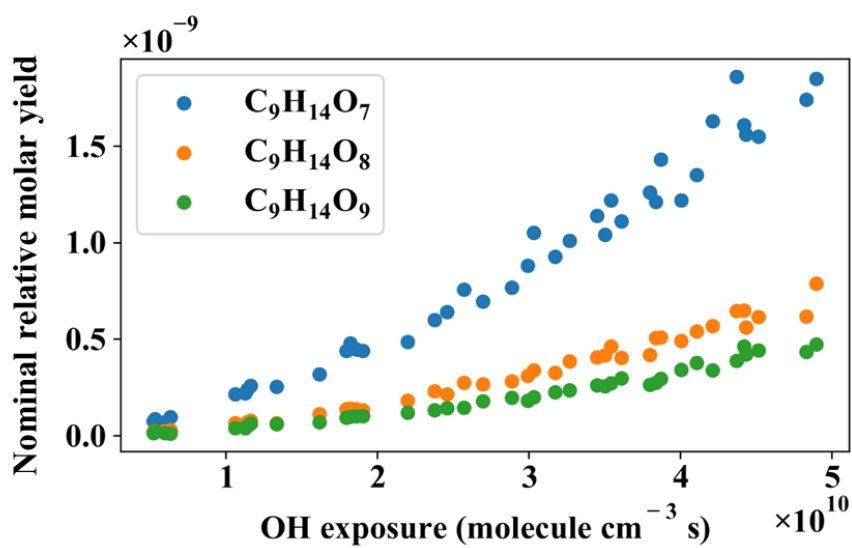
Figure 3b
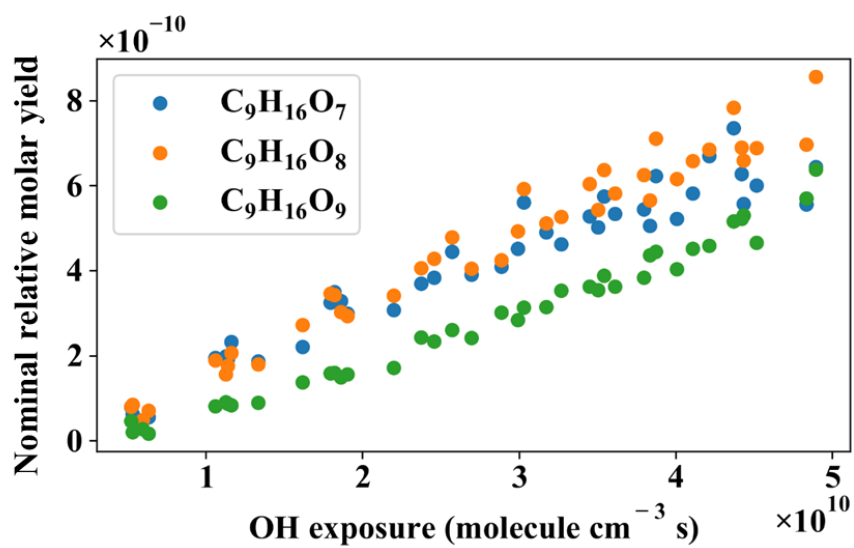
Figure 3c
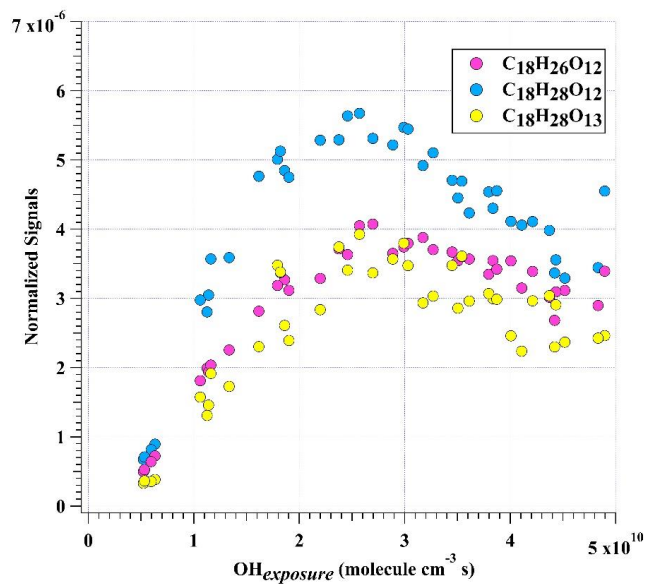
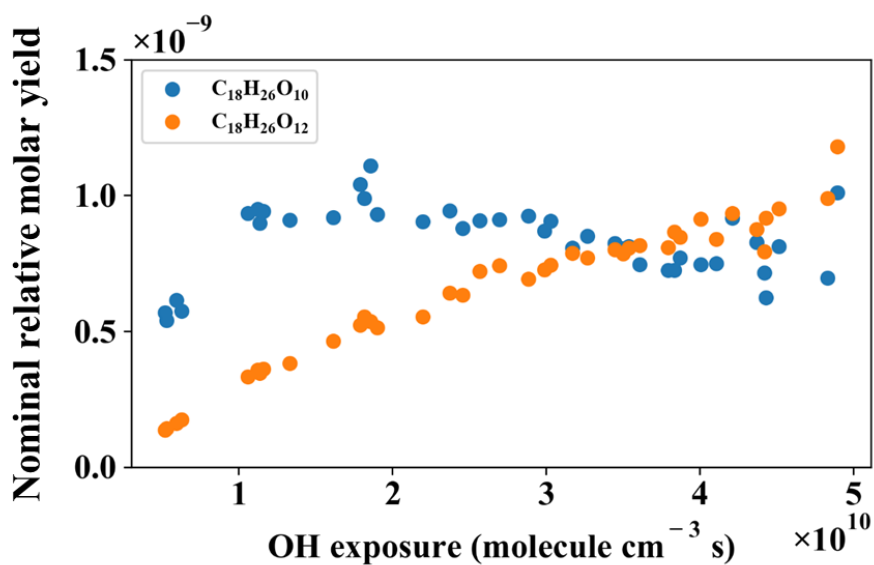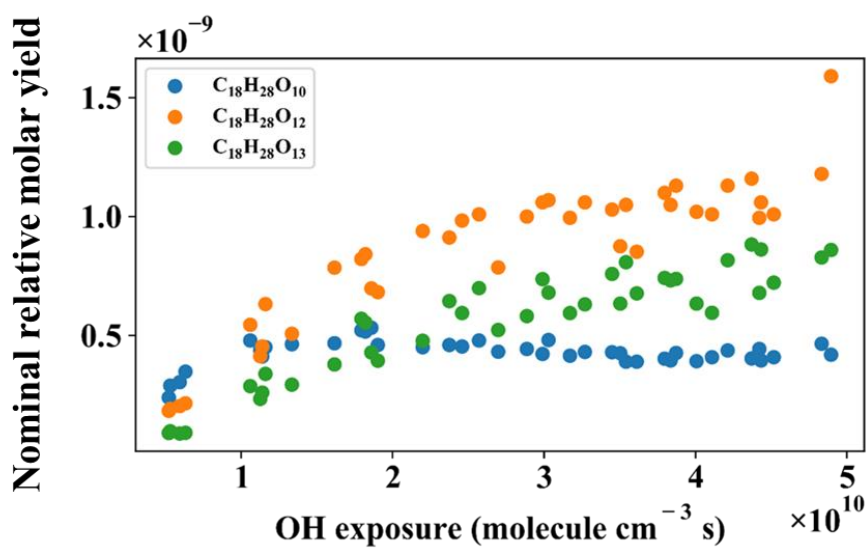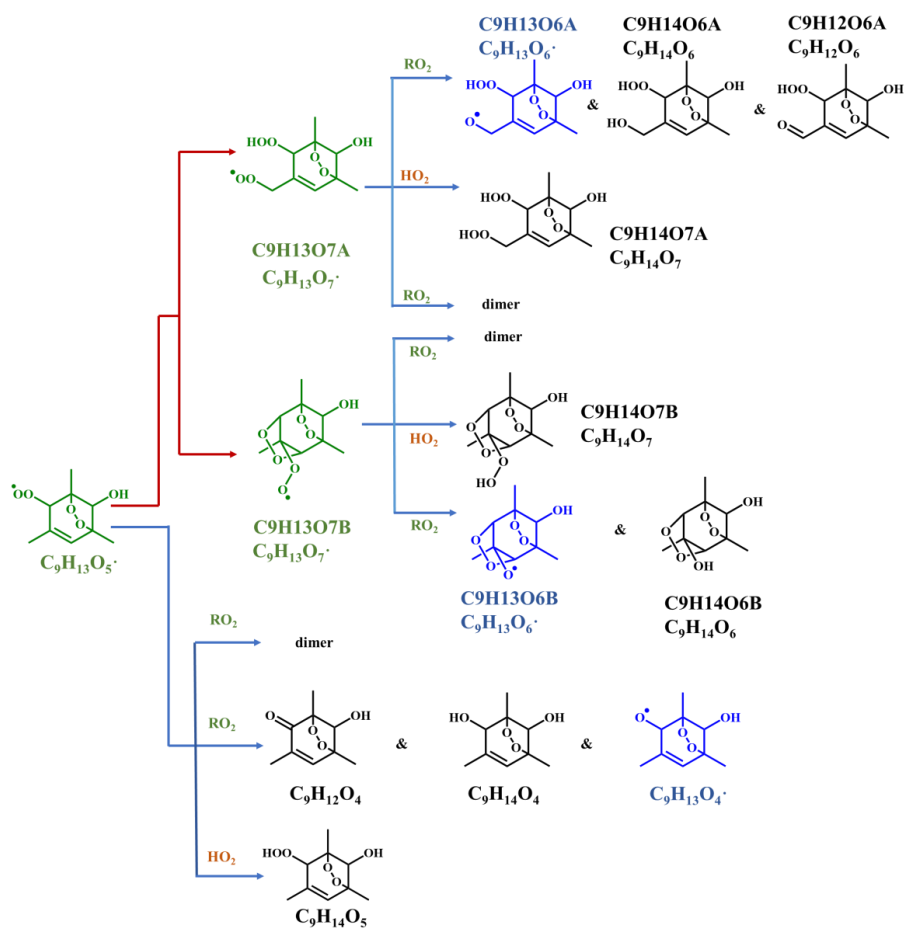**Figure 4a**
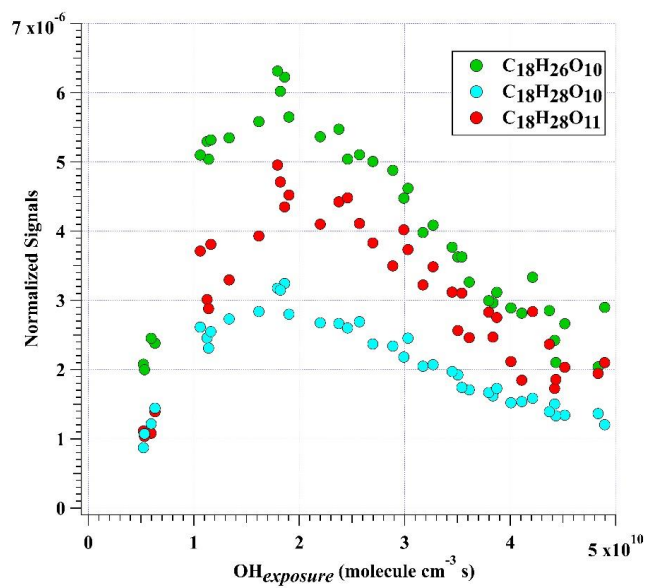
Figure 4b

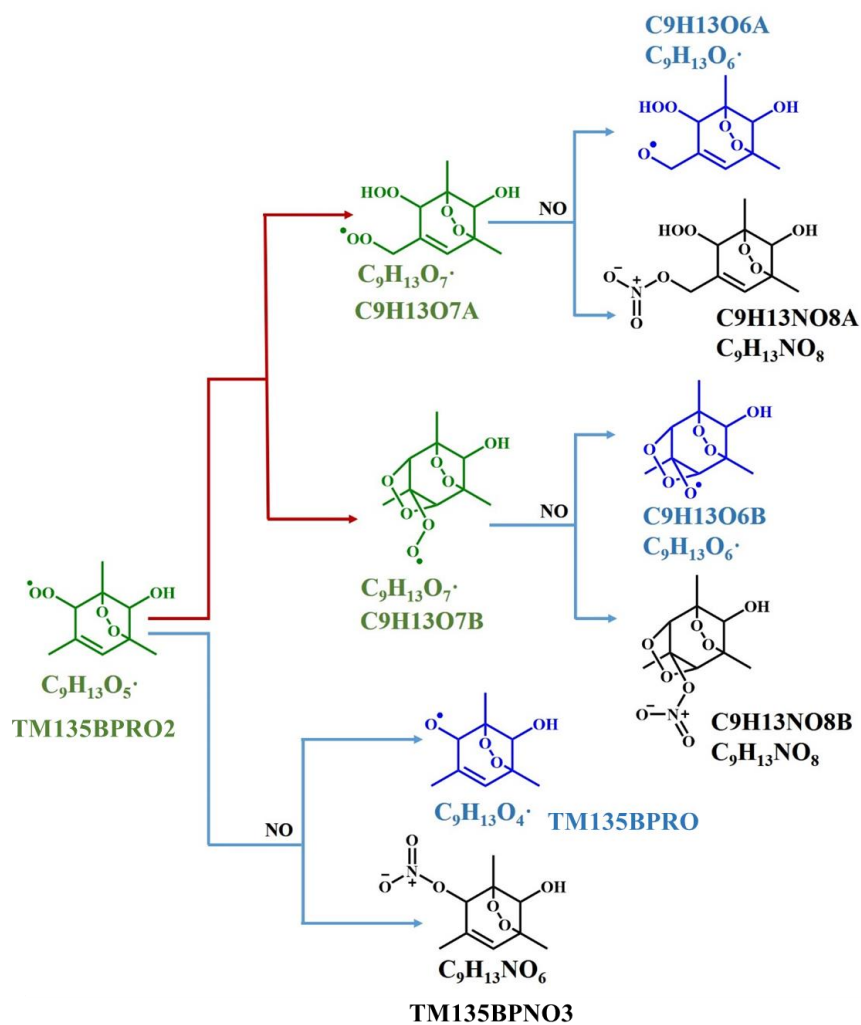**Figure 5a**

Figure 5b

Scheme Captions

Scheme 1. Oxidation pathways of the bicyclic peroxy radical $C_9H_{13}O_5\cdot$ (MCM name: TM135BPRO2) in the OH-initiated oxidation of 1,3,5-TMB. Green, blue, and black formulae denote alkyl peroxy radicals, alkoxy radicals and stabilized products, respectively. Red arrows denote the autoxidation pathway. MCM names for HO_2- and RO_2-termination products of TM135BPRO2 are present, whereas MCM names for termination products of $C_9H_{13}O_7\cdot$ are unavailable and thus named according to the autoxidation intermediates.

Scheme 2. NO termination reactions of the bicyclic peroxy radical $C_9H_{13}O_5\cdot$ (MCM name: TM135BPRO2) and its autoxidation reaction products. Green, blue, and black formulae denote alkyl peroxy radicals, alkoxy radicals and stabilized products, respectively. Red arrows denote the autoxidation pathway. MCM names of NO-termination products of TM135BPRO2 are present, whereas MCM names for termination products of $C_9H_{13}O_7\cdot$ are unavailable and thus named according to the autoxidation intermediates.

Scheme 1

Scheme 2